Computer Assisted Mechanics and Engineering Sciences, 15: 337–351, 2008.

Application of the Wave Based Technique for steady-state semi-infinite sound radiation analysis

Jan Rejlek[1], Bert Pluymers[2], Achim Hepberger[1], Hans-Herwig Priebsch[1], Wim Desmet[2]

[1] *Virtual Vehicle Competence Center (vif)*
(Former ACC – Acoustic Competence Centre Graz)
Inffeldgasse 21/A, A-8010, Graz, Austria

[2] *Katholieke Universiteit Leuven, Department of Mechanical Engineering*
Celestijnenlaan 300 B, B-3001, Heverlee, Belgium

(Received in the final form November 5, 2008)

This paper reports on the development of a novel wave based prediction technique for the steady-state sound radiation analysis of three-dimensional semi-infinite problems. Instead of simple polynomial shape functions, this method adopts an indirect Trefftz approach, in which it uses the exact solutions of the governing differential equation for the field variables approximation. Since a fine discretization is no longer required, the resulting wave based models are substantially smaller than the element-based counterparts. Application of the proposed approach to various validation examples illustrates an enhanced computational efficiency as compared with element-based methods.

1. Introduction

In several engineering areas, methodologies based on the Trefftz approach [13] have received a significant recognition over the last decades [10]. The main reason for rediscovering the Trefftz methods consists in the fact that they use the exact solutions of the governing differential equation for the field variables approximation. Especially when solving problems exhibiting a wave-like nature, such as acoustics, structural dynamics or electromagnetic problems, this becomes a major advantage in contrast to the conventional element-based methods.

In the recent years, the wave based prediction technique (WBT) [4] has been developed as an alternative method for solving steady-state acoustic problems. The method adopts an indirect Trefftz approach by incorporating a priori knowledge of the solved problem. Instead of simple polynomial shape functions, the exact solutions of the governing differential equation are employed to approximate the dynamic phenomena. As a result, fine element discretization is no longer needed which yields smaller numerical models that exhibit an enhanced computational efficiency as compared with element-based methods.

The WBT has proven to be a robust prediction tool for interior acoustics [7]. However, a considerable class of real-life acoustic applications involves the analysis of problems in unbounded domains, such as sound scattering or sound radiation problems. This kind of problems poses a real challenging task since the unbounded region is not admissible for any direct discretization and requires some additional treatment. Various strategies were developed in order to tackle the unbounded problems using the standard finite element schemes, such as non-reflecting boundary condition [6], infinite elements [1] or perfectly matched layers [2]. All these concepts, although based on different approaches, have the same basic idea in common, namely, introducing an artificial truncation boundary that divides the infinite domain into two regions – a bounded and unbounded one.

Recently, the WBT has also been applied for two-dimensional (2D) unbounded [9, 11] and semi-infinite problems [3]. This paper discusses the application of the WBT for a three-dimensional (3D) analysis of semi-infinite radiation problems. The conventional wave based interior formulation is used in the bounded part, while some new additional functions, which inherently satisfy the Sommerfeld radiation condition and take the infinite rigid baffle into account, are applied in the unbounded part of the wave based model. Both, the analytical solution and the numerical results are used to demonstrate the performance of the proposed approach.

2. Problem definition

Consider an unbounded three-dimensional acoustic problem as shown in Fig. 1(a). The problem consist of a closed boundary surrounded by fluid characterized by its speed of sound c and the density ρ. Assuming that the system is linear, the fluid is inviscid and the process adiabatic, the steady-state pressure response $p(\mathbf{r},t) = p(\mathbf{r})e^{j\omega t}$ at an arbitrary position $\mathbf{r}$ within the solution domain Ω is governed by the homogeneous Helmholtz equation

$$\triangle p(\mathbf{r}) + k^2 p(\mathbf{r}) = 0, \tag{1}$$

where $\triangle \equiv \frac{\partial^2}{\partial x^2} + \frac{\partial^2}{\partial y^2} + \frac{\partial^2}{\partial z^2}$ represents the Laplace operator in Cartesian coordinates, $\mathbf{r}$ the position vector, t the time, $j = \sqrt{-1}$ the imaginary unit, ω the circular frequency and $k = \omega/c$ the wave number.

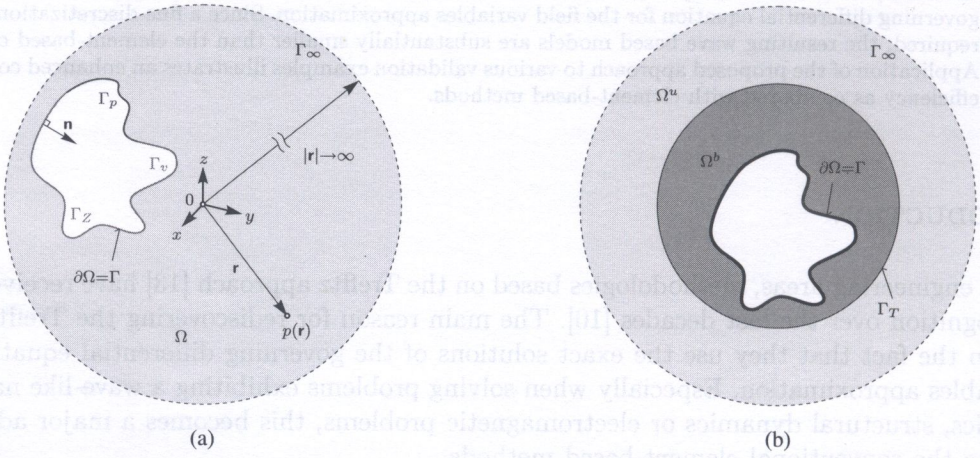

Fig. 1. (a) An unbounded 3D acoustic problem and (b) the concept of the truncation boundary Γ_T

Since the Helmholtz equation (1) is a second-order partial differential equation, one boundary condition has to be specified at each point of the boundary in order to be the problem well-posed. At the problem boundary $\partial\Omega = \Gamma$ three following types of boundary condition forming a non-overlapping set $\Gamma = \Gamma_p \cup \Gamma_v \cup \Gamma_Z$ may be imposed:

- pressure boundary condition (Dirichlet)

$$\mathbf{r} \in \Gamma_p : \ \hat{p}(\mathbf{r}) = \bar{p}(\mathbf{r}), \tag{2}$$

- normal velocity boundary condition (Neumann)

$$\mathbf{r} \in \Gamma_v : \ \mathcal{L}_v(\hat{p}(\mathbf{r})) = \frac{j}{\rho\omega}\frac{\partial \hat{p}(\mathbf{r})}{\partial n} = \bar{v}_n(\mathbf{r}), \tag{3}$$

- normal impedance boundary condition (mixed)

$$\mathbf{r} \in \Gamma_Z : \; \mathcal{L}_Z(\hat{p}(\mathbf{r})) = \mathcal{L}_v(\hat{p}(\mathbf{r})) - \frac{\hat{p}(\mathbf{r})}{\bar{Z}_n(\mathbf{r})} = 0, \tag{4}$$

with $\frac{\partial}{\partial n}$ the normal derivative and $\bar{p}(\mathbf{r})$, $\bar{v}_n(\mathbf{r})$ and $\bar{Z}_n(\mathbf{r})$ the prescribed values of the acoustic pressure, normal velocity and normal impedance.

Moreover, as the solution domain Ω is unbounded, an additional Sommerfeld radiation condition has to be imposed at Γ_∞ in order to ensure, that no acoustic energy reflections occur at the infinity

$$\lim_{|\mathbf{r}|\to\infty} \left[|\mathbf{r}| \left(\frac{\partial p(\mathbf{r})}{\partial |\mathbf{r}|} + \mathrm{j}kp(\mathbf{r}) \right) \right] = 0. \tag{5}$$

3. Wave Based Technique

The WBT [4] is based on indirect Trefftz approach, in which it incorporates an a priori knowledge of the solved problem. The field variables are expressed in terms of globally defined shape functions, which are the exact solutions of the homogeneous governing differential equation (1), but which may violate the boundary conditions (2)–(4). In the wave based formulation for interior problems [7], these functions represent evanescent and propagating plane waves and form the wave function set $\mathbf{\Phi}^b(\mathbf{r})$. Using a weighted residual scheme, the residual errors arising at the boundary are enforced to zero in an integral sense. Solution of the resulting system of algebraic equations yields the contribution factors of the wave functions. The wave models are substantially smaller than equivalent Finite Element (FE) [14] and Boundary Element (BE) [5] models and exhibit an increased computation efficiency.

In order to tackle the problems involving unbounded domains, an additional treatment of the interior WB formulation is required [8]. By introducing an artificial truncation boundary Γ_T, see Fig. 1(b), the solution domain Ω is divided into a bounded and unbounded part $\Omega = \Omega^b + \Omega^u$. In the bounded part, the WB formulation for interior problems can be applied [4, 8], whereas, in the unbounded part, functions which additionally satisfy the Sommerfeld radiation condition (5), are employed [9].

3.1. Bounded domain

Within the bounded part of the wave model, a linear combination of the shape functions approximates the exact pressure solution

$$p^b(\mathbf{r}) \approx \hat{p}^b(\mathbf{r}) = \sum_{i=1}^{M} p_i^b \Phi_i^b(\mathbf{r}) = \mathbf{\Phi}^b(\mathbf{r})\, \mathbf{p}^b, \tag{6}$$

with $\mathbf{\Phi}^b(\mathbf{r})$ the wave function set

$$\mathbf{\Phi}^b(\mathbf{r}) = \begin{cases} \Phi_r(x,y,z) = \cos(k_{rx}x)\, \cos(k_{ry}y)\, \mathrm{e}^{-\mathrm{j}k_{rz}z} \\ \Phi_s(x,y,z) = \cos(k_{sx}x)\, \mathrm{e}^{-\mathrm{j}k_{sy}y}\, \cos(k_{sz}z) \\ \Phi_t(x,y,z) = \mathrm{e}^{-\mathrm{j}k_{tx}x}\, \cos(k_{ty}y)\, \cos(k_{tz}z) \end{cases} \tag{7}$$

and p_i^b the M unknown contribution factors forming the interior degrees of freedom,

$$M = \dim \mathbf{\Phi}^b = 2(n_r+1)^2 + 2(n_s+1)^2 + 2(n_t+1)^2. \tag{8}$$

Each function in the set (7) is an exact solution of the homogeneous Helmholtz equation (1). Since the only requirement for the wave number components in Eq. (7) is that

$$k_{rx}^2 + k_{ry}^2 + k_{rz}^2 = k_{sx}^2 + k_{sy}^2 + k_{sz}^2 = k_{tx}^2 + k_{ty}^2 + k_{tz}^2 = k^2, \tag{9}$$

an infinte number of wave functions (7) can be defined for the expansion (6). The wave number components are selected as follows [4],

$$k_{r\bullet} = \begin{cases} k_{rx} = \dfrac{r\pi}{L_x}, & r = 0, 1, 2, \ldots, n_r \\ k_{ry} = \dfrac{r\pi}{L_y} \\ k_{rz} = \pm\sqrt{k^2 - k_{rx}^2 - k_{ry}^2}, \end{cases} \tag{10}$$

$$k_{s\bullet} = \begin{cases} k_{sx} = \dfrac{s\pi}{L_x}, & s = 0, 1, 2, \ldots, n_s \\ k_{sy} = \pm\sqrt{k^2 - k_{sx}^2 - k_{sx}^2} \\ k_{sz} = \dfrac{s\pi}{L_z}, \end{cases} \tag{11}$$

$$k_{t\bullet} = \begin{cases} k_{tx} = \pm\sqrt{k^2 - k_{ty}^2 - k_{tz}^2} \\ k_{ty} = \dfrac{t\pi}{L_y}, & t = 0, 1, 2, \ldots, n_t \\ k_{tz} = \dfrac{t\pi}{L_z}. \end{cases} \tag{12}$$

The integer sets r, s and t determine the M degrees of freedom of the interior model and L_x, L_y and L_z are the dimensions of the smallest rectangular domain, enclosing the considered problem domain. Desmet [4] proves that the solution approximation (6) converges towards exact solution for $M \to \infty$, provided that the solution domain is convex. If the considered problem domain is non-convex, a partitioning into non-overlapping convex subdomains is required. At the coupling interface Γ_i between two subdomains continuity conditions must be imposed [8],

$$\frac{\mathrm{j}}{\rho\omega}\frac{\partial p_1(\mathbf{r}_1)}{\partial n_1} - \frac{p_1(\mathbf{r}_1)}{\bar{Z}_{int}} = -\frac{\mathrm{j}}{\rho\omega}\frac{\partial p_2(\mathbf{r}_2)}{\partial n_2} - \frac{p_2(\mathbf{r}_2)}{\bar{Z}_{int}}, \qquad \mathbf{r}_{1,2} \in \Gamma_i, \tag{13}$$

$$\frac{\mathrm{j}}{\rho\omega}\frac{\partial p_2(\mathbf{r}_2)}{\partial n_2} - \frac{p_2(\mathbf{r}_2)}{\bar{Z}_{int}} = -\frac{\mathrm{j}}{\rho\omega}\frac{\partial p_1(\mathbf{r}_1)}{\partial n_1} - \frac{p_1(\mathbf{r}_1)}{\bar{Z}_{int}}, \qquad \mathbf{r}_{1,2} \in \Gamma_i, \tag{14}$$

where n_1, n_2 are the outward oriented normal vectors and $\bar{Z}_{int} = \rho c$ is the internal impedance which equals to the characteristic impedance.

3.2. Unbounded domain

Apart from the Helmholtz equation (1), the pressure approximation for the unbounded domain has to satisfy the Sommerfeld radiation condition (5), in addition. The following pressure solution expansion complies with these requirements and converges for $L \to \infty$,

$$p(r, \vartheta, \varphi) \approx \sum_{l=0}^{L} \sum_{m=-l}^{l} p_{lm}^u \, h_l^{(2)}(kr) \, \mathrm{Y}_l^m(\vartheta, \varphi), \tag{15}$$

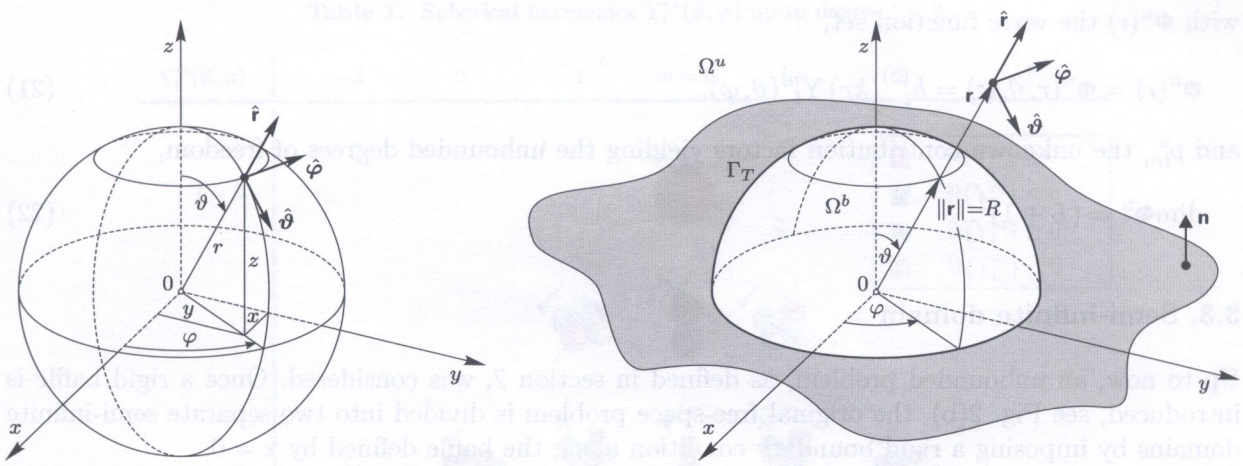

Fig. 2. (a) Spherical coordinate system and (b) an introduction of the rigid baffle

with r, φ and ϑ the radial, azimuthal and zenithal spherical coordinates according to Fig. 2(a) with the following transformation formulas,

$$\begin{aligned} x &= r \sin\vartheta \cos\varphi, \\ y &= r \sin\vartheta \sin\varphi, \\ z &= r \cos\vartheta, \end{aligned} \tag{16}$$

to the Cartesian coordinates x, y, z. This convention will be used throughout the paper. In Fig. 2(a) $\hat{\mathbf{r}}$, $\hat{\boldsymbol{\varphi}}$ and $\hat{\boldsymbol{\vartheta}}$ are the unit vectors in the spherical coordinates. In solution expansion (15) $h_l^{(2)}(kr)$ is the spherical Hankel function of the second kind,

$$h_l^{(2)}(kr) = \sqrt{\frac{\pi}{2kr}}\, \mathrm{H}^{(2)}_{l+\frac{1}{2}}(kr), \tag{17}$$

representing the radial decay function, and $\mathrm{Y}_l^m(\vartheta, \varphi)$ are the spherical harmonics,

$$\mathrm{Y}_l^m(\vartheta, \varphi) = \sqrt{\frac{2l+1}{4\pi}\frac{(l-m)!}{(l+m)!}}\, \mathrm{P}_l^m(\cos\vartheta) \mathrm{e}^{\mathrm{j}m\varphi}, \tag{18}$$

which correspond to the angular portion of the differential equation solution. In the spherical harmonics (18) $\mathrm{P}_l^m(\cos\vartheta)$ is the associated Legendre polynomial. In the following, the identity

$$\mathrm{Y}_l^{-m}(\vartheta, \varphi) = (-1)^m\, \overline{\mathrm{Y}}_l^m(\vartheta, \varphi) \tag{19}$$

is used for $m < 0$. Expansion (15) may be rewritten in an analogous way as the pressure approximation in the bounded part of wave model (6),

$$p^u(\mathbf{r}) \approx \hat{p}^u(\mathbf{r}) = \sum_{l=0}^{L} \sum_{m=-l}^{l} p^u_{lm}\, \Phi^u_i(\mathbf{r}) = \boldsymbol{\Phi}^u(\mathbf{r})\, \mathbf{p}^u, \tag{20}$$

with $\mathbf{\Phi}^u(\mathbf{r})$ the wave function set,

$$\mathbf{\Phi}^u(\mathbf{r}) = \mathbf{\Phi}^u(r,\vartheta,\varphi) = h_l^{(2)}(kr)\,\mathrm{Y}_l^m(\vartheta,\varphi), \tag{21}$$

and p_{lm}^u the unknown contribution factors yielding the unbounded degrees of freedom,

$$\dim\mathbf{\Phi}^u = (L+1)^2. \tag{22}$$

3.3. Semi-infinite domain

Up to now, an unbounded problem, as defined in section 2, was considered. Once a rigid baffle is introduced, see Fig. 2(b), the original free-space problem is divided into two separate semi-infinite domains by imposing a rigid boundary condition along the baffle defined by $z = 0$,

$$\left.\frac{\partial p(\mathbf{r})}{\partial n}\right|_{\vartheta=\frac{\pi}{2},\, r\geq 0} = 0. \tag{23}$$

In order to take the baffle into account, wave functions used in the unbounded part of the wave model have to incorporate the rigid boundary condition (23), inherently. The selection of appropriate functions starts from the original full-space functions (21). Expressing solution expansion (15) for the particular case when a response point coincides with the baffle,

$$\left.\frac{\partial p(\mathbf{r})}{\partial \vartheta}\right|_{\vartheta=\frac{\pi}{2},\, r\geq R} = \sum_{l=0}^{L}\sum_{m=-l}^{m=l} \underbrace{p_{lm}^u\, h_l^{(2)}(kr)\sqrt{\frac{2l+1}{2\pi}\frac{(l-|m|)!}{(l+|m|)!}}\,\mathrm{e}^{\mathrm{j}m\varphi}}_{\neq f(\vartheta)}\ \underbrace{\mathrm{P}_l^{'|m|}(\cos\vartheta)}_{\stackrel{!}{=}0} = 0, \tag{24}$$

one may cluster all terms not depending on the zenithal coordinate ϑ[1] and isolate the zenith-dependent part of the expression, which is only the derivative of an associated Legendre polynomial with respect to ϑ. Since the first term of the expression (24) does not depend on ϑ, only the derivative of the associated Legendre polynomial $\mathrm{P}_l^{'m}(0)$ must equal to zero in order to satisfy the condition (23). From the properties of the associated Legendre polynomials [12]

$$\mathrm{P}_l^{'m}(0) = \begin{cases} 0, & l+m = \text{even}, \\ (-1)^{\left(\frac{l+m-1}{2}\right)}\dfrac{1\cdot 3\cdot 5\ldots(l+m)}{2\cdot 4\cdot 6\ldots(l-m-1)}, & l+m = \text{odd}, \end{cases} \tag{25}$$

only the spherical harmonics with a $(l+m = \text{even})$ combination satisfy the baffle condition (23). As a result, the even configurations are retained in the wave function set, while those with an odd shape are taken out of the set. Obviously, the size of the original full-space wave function set (21) will be reduced by removing the odd $\mathrm{Y}_l^m(\vartheta,\varphi)$ components. Table 1 captures the spherical harmonics up to degree $l = 3$ and the corresponding orders $m = -l, -l+1, \ldots, l-1, +l$ plotted as directional characteristics for various azimuths φ and zeniths ϑ. In the diagrams red and blue colors denote the positive and negative values of the real part of Y_l^m and similarly green and yellow colors represent positive and negative values of the imaginary part of Y_l^m, respectively. Functions with an even configuration forming the semi-infinite wave function set $\mathbf{\Phi}^{si}$ are labeled with checkmarks ✓, whereas those tagged with crosses × (odd ones) are removed, which yields a reduces size of the set

$$\dim\mathbf{\Phi}^{si} = \frac{(L+1)(L+2)}{2}. \tag{26}$$

[1] As the baffle was introduced into the problem, the normalization factor became 2π corresponding to a solid angle of the semi-infinite space.

Table 1. Spherical harmonics $\mathrm{Y}_l^m(\vartheta, \varphi)$ up to degree $l = 3$

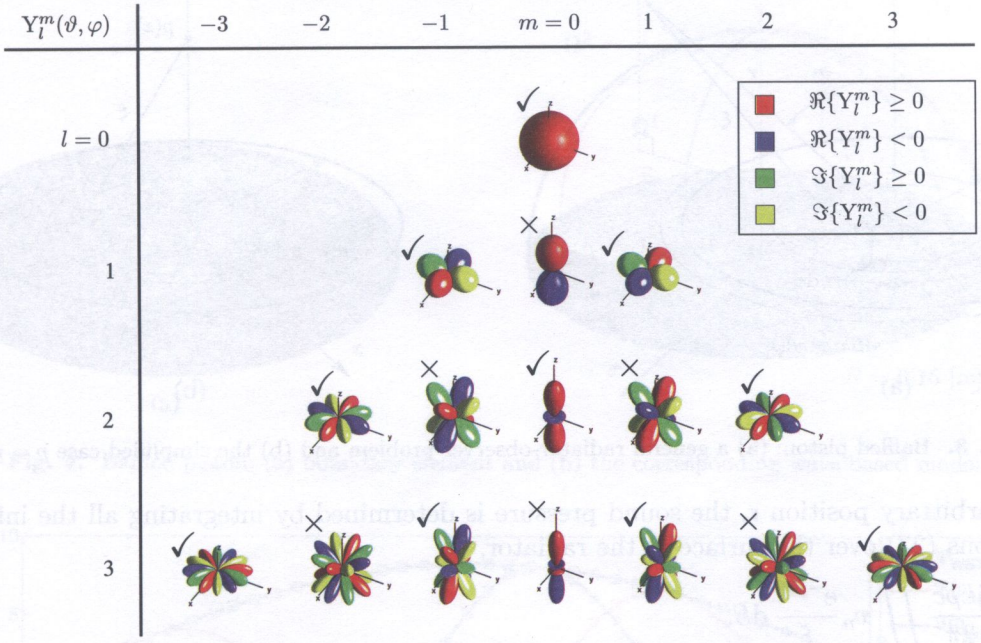

4. Validation examples

To illustrate the performance of the proposed wave based approach, two different validation examples are presented in this section. While the first one considers a comparison of the WB results with both an analytical as well as with a BE solution, the second validation is only based on a numerical BE solution. All calculations are performed on a 3 GHz single core Intel based system using 1 Gbyte RAM and running the Windows 2000 operating system.

4.1. Baffled piston

The first validation example represents a circular piston radiator of radius $R = 0.15\,[\mathrm{m}]$ mounted in an infinite rigid baffle, see Fig. 3(a). Assuming a piston-like vibrational behavior, all points forming the surface of the radiator are vibrating in phase with a normal velocity of $v_n = 0.01\ [\mathrm{m/s}]$. The surrounding fluid is considered to be air with the following material properties: $c = 343.8\,[\mathrm{m/s}]$, $\rho = 1.2\,[\mathrm{kg/m^3}]$.

4.1.1. Analytical solution

For problems considering single or multiple planar radiators mounted in a rigid baffle the sound radiation phenomena may be investigated by evaluating the Rayleigh integral. In terms of differential calculus, each point on the surface of the radiator represents an elementary sound source corresponding to an infinitesimal pressure contribution

$$\mathrm{d}p(\xi) = \frac{\mathrm{j}k\rho c v_n}{2\pi} \frac{\mathrm{e}^{-\mathrm{j}k\xi}}{\xi} \mathrm{d}S \tag{27}$$

to the overall sound pressure at a distance ξ. ξ is measured between the infinitesimal radiating surface $\mathrm{d}S$ laying on the radiator and the field point $\mathbf{r}$ located within the investigated semi-infinite domain above the baffle plane ($z > 0$),

$$\xi = \sqrt{r^2 + \varrho^2 - 2r\varrho \sin\vartheta \cos(\phi - \varphi)}. \tag{28}$$

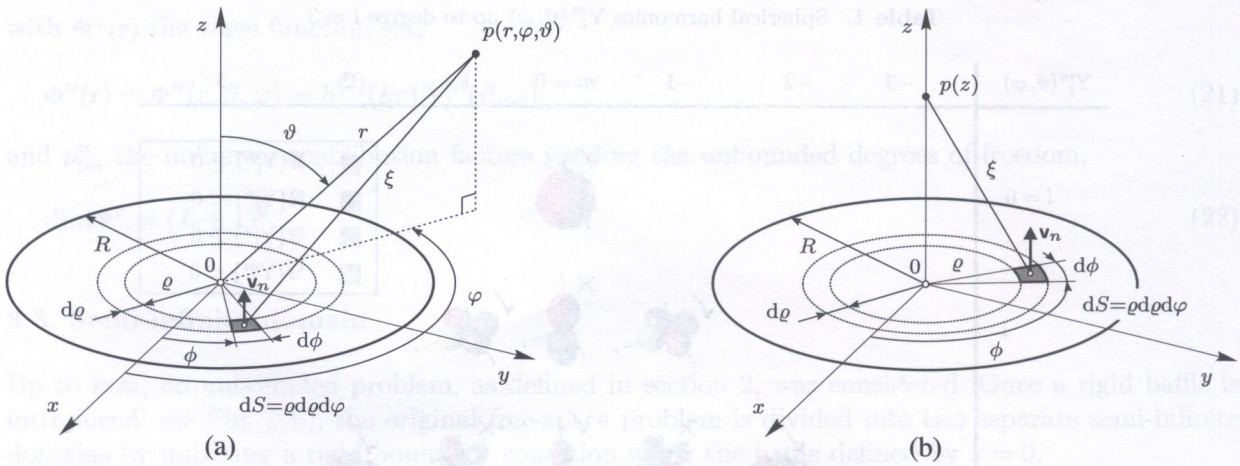

Fig. 3. Baffled piston: (a) a general radiator-observer problem and (b) the simplified case $p = p(z)$

At an arbitrary position $\mathbf{r}$, the sound pressure is determined by integrating all the infinitesimal contributions (27) over the surface of the radiator,

$$p(\mathbf{r}) = \frac{\mathrm{j}k\rho c}{2\pi} \iint_S v_n \frac{\mathrm{e}^{-\mathrm{j}k\xi}}{\xi} \,\mathrm{d}S, \tag{29}$$

yielding the aforementioned Rayleigh integral. As the integrand of the Rayleigh integral (29) depends on both the position of the elementary source $\mathrm{d}S = \varrho \mathrm{d}\varrho \mathrm{d}\varphi$ as well as the field point $\mathbf{r}$, solution of the general case involves an infinite series expansion. However, a significant simplification of the original problem can be made by reducing it to an axisymmetrical problem, as depicted in Fig. 3(b). Since the pressure depends only on the z-coordinate, the expression for the radiator-observer distance ξ becomes

$$\xi = \sqrt{\varrho^2 + z^2}. \tag{30}$$

Furthermore, by taking the piston-like vibrational behavior into account, the evaluation of the Rayleigh integral (29) can be carried out in a straightforward way resulting in an analytical closed-form solution,

$$p(z) = \frac{\mathrm{j}k\rho c v_n}{2\pi} \int_0^R \underbrace{\int_0^{2\pi} \frac{\mathrm{e}^{-\mathrm{j}k\xi}}{\xi} \mathrm{d}\phi}_{=2\pi} \varrho \mathrm{d}\varrho = \mathrm{j}k\rho c v_n \int_z^{\sqrt{R^2+z^2}} \mathrm{e}^{-\mathrm{j}k\xi} \mathrm{d}\xi = \rho c v_n \left[\mathrm{e}^{-\mathrm{j}kz} - \mathrm{e}^{-\mathrm{j}k\sqrt{R^2+z^2}}\right]. \tag{31}$$

4.1.2. Numerical models

The computational mesh used in the involved BE model consists of 4729 nodes forming 9216 triangular linear acoustic elements, as shown in Fig. 4(a). For the BE calculations the LMS/Sysnoise Rev. 5.5 simulation software is used by applying a baffled direct collocational scheme.

According to the problem definition a corresponding WB model is constructed. As the radius of the truncation hemisphere Γ_T is chosen to coincide with the radius of the piston R, the resulting wave model consists only of one convex Ω^1 and one semi-infinite domain Ω^2, see Fig. 4(b). The bounded part consists of 294 degrees of freedom (wave functions), while in the semi-infinite region 28 wave functions are applied. The WBT routines are implemented in MATLAB.

4.1.3. Frequency response analysis

For the frequency response evaluations two response points are selected: $\mathbf{r}_1 = (0; 0; 0.1)$ [m] located in the bounded part of the WB model and $\mathbf{r}_2 = (0; 0; 1)$ [m] outside the truncation hemisphere Γ_T

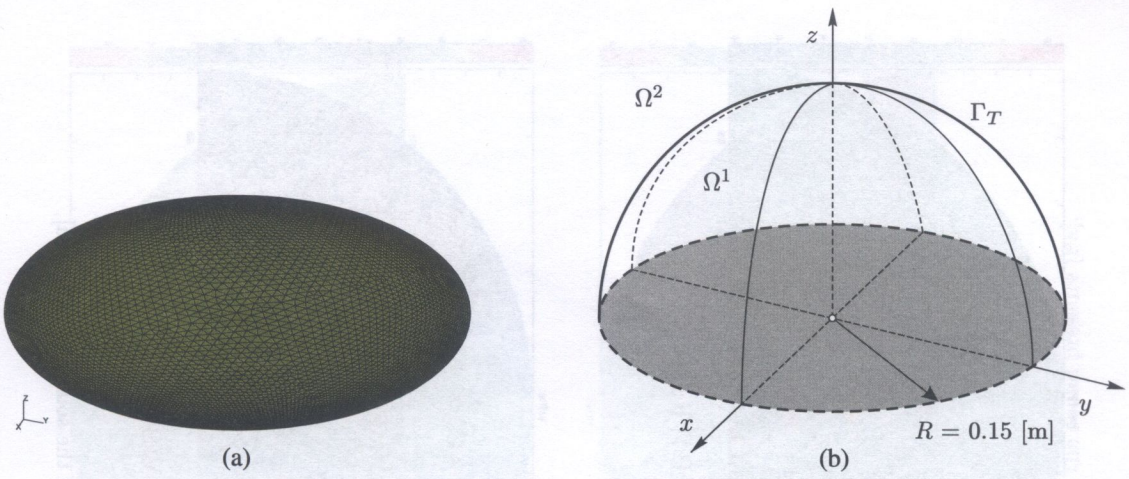

Fig. 4. Baffled piston: (a) boundary element and (b) the corresponding wave based model

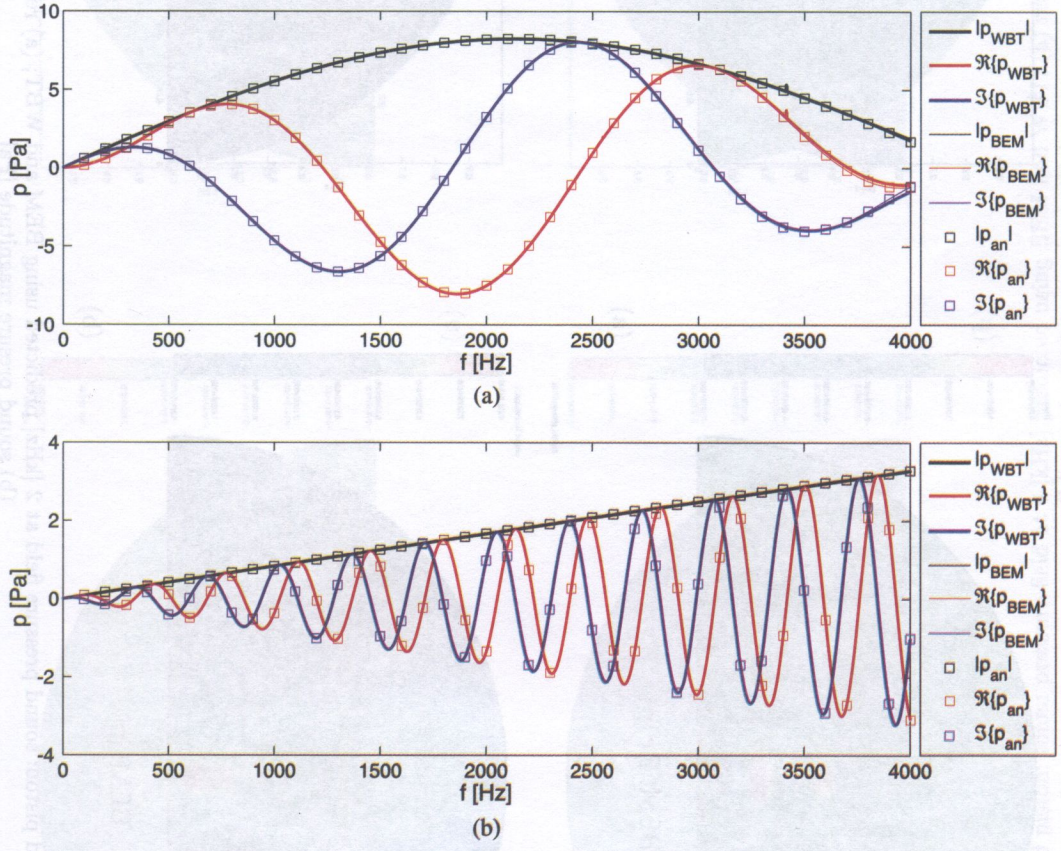

Fig. 5. Baffled piston: sound pressure responses up to 4 [kHz] evaluated at (a) $\mathbf{r}_1$ and (b) $\mathbf{r}_2$

within the semi-infinite domain. Figure 5 plots the response spectra for the sound pressure calculated by the analytical formula (31) and by both BE and WB approaches at response point (a) $\mathbf{r}_1$ and (b) $\mathbf{r}_2$, respectively. Similarly, Figs. 6 and 7 show the pressure field in the proximity of the radiator plotted on a slice perpendicular to the baffle plane at 2 [kHz] and 4 [kHz], respectively. For the contour plots of the BE and WB results the same color scaling is used. The black solid line in the right hand side contour plots indicates the truncation hemisphere Γ_T as used in the WB model.

Figures 5, 6 and 7 illustrate a good agreement between the WB and BE predictions in a wide frequency range.

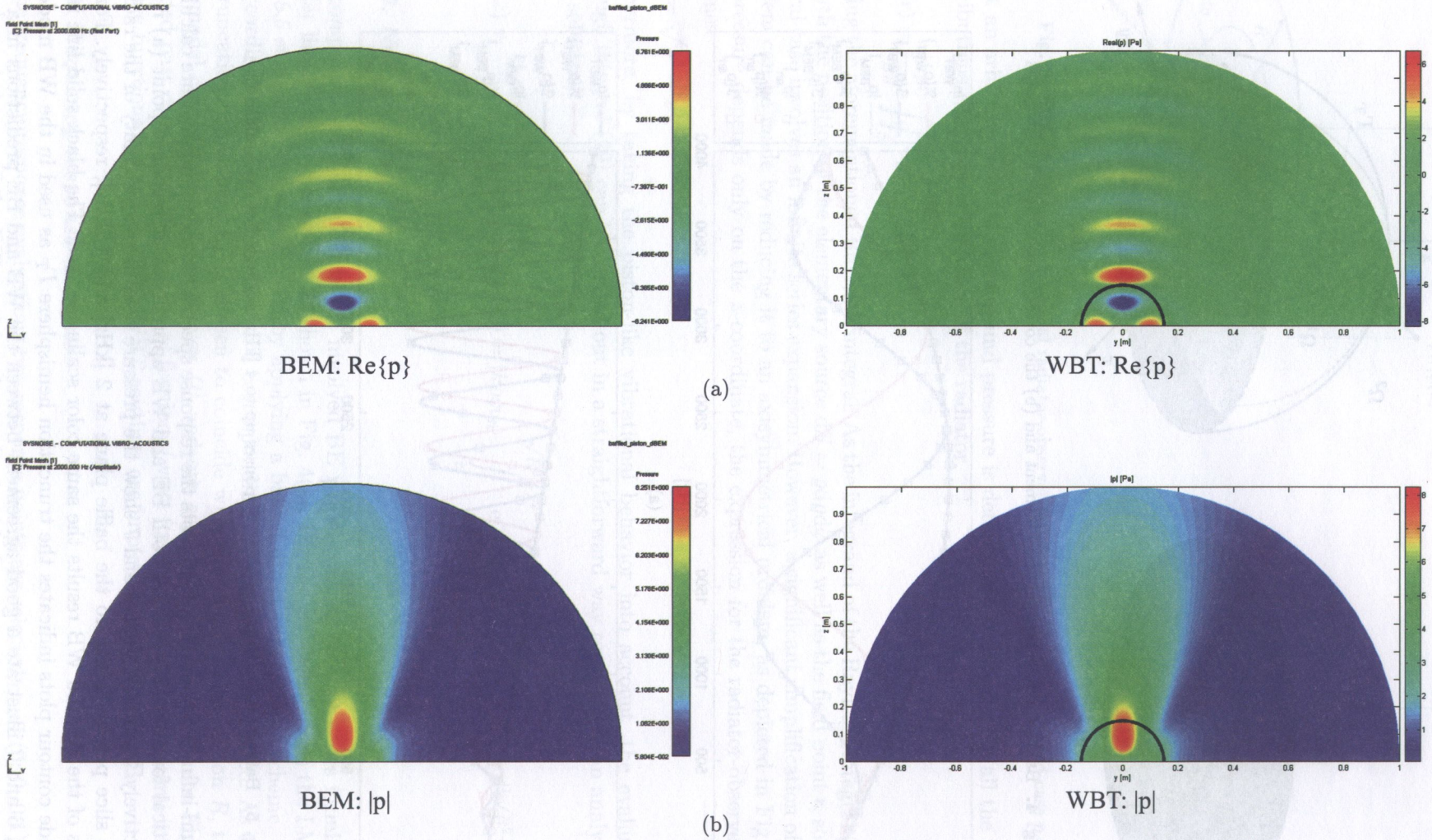

Fig. 6. Baffled piston: sound pressure field at 2 [kHz] predicted using BEM and WBT; (a) real part of the sound pressure [Pa], (b) sound presure magnitude [Pa]

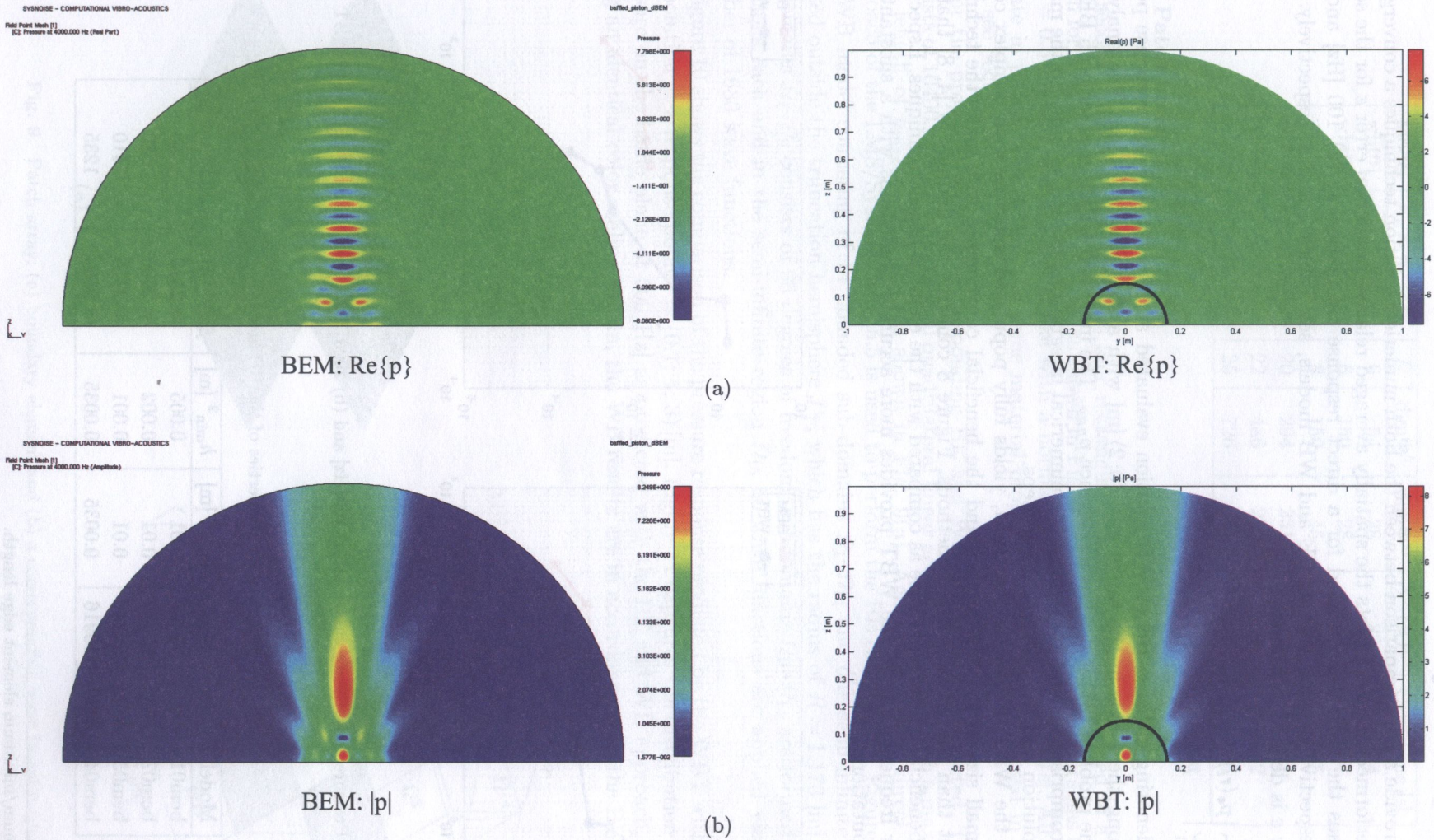

Fig. 7. Baffled piston: sound pressure field at 4 [kHz] predicted using BEM and WBT; (a) real part of the sound pressure [Pa], (b) sound presure magnitude [Pa]

4.1.4. Convergence analysis

In order to provide a fair comparison between the both numerical solution techniques a convergence analysis is performed. Figure 8 plots the spatially averaged relative prediction error ε for the sound pressure versus the CPU time needed for a direct response calculation at (a) 100 [Hz] and (b) 2000 [Hz], respectively, using various BE and WB models, see Tables 2 and 3, respectively. The relative error ε is defined as follows,

$$\varepsilon = \frac{1}{N} \sum_{i=1}^{N} \left| \frac{p_\bullet(\mathbf{r}_i) - p_{REF}(\mathbf{r}_i)}{p_{REF}(\mathbf{r}_i)} \right|, \tag{32}$$

with $p_\bullet(\mathbf{r}_i)$ denoting either a BE or WB solution evaluated at $N = 21$ different response points $\mathbf{r}_i$ located along the z-axis in the range $z = \langle 0; 2 \rangle$ [m] with a step size of 0.1 [m]. The analytical solution of the problem (31) is used as a reference p_{REF}. The indicated CPU times for both BE and WB models comprise the time to perform the numerical integrations needed to built up the matrix system, its solution and the postprocessing steps.

Although the WBT, similar as the BEM, yields fully populated matrices with complex coefficients, the small size of the WB models and the beneficial convergence rate make the technique more efficient than the element-based methods. Figure 8 confirms the findings of [4, 8] that the WBT has a beneficial convergence rate as compared with the element-based techniques. Especially, in the higher frequency range, the WBT provides more accurate predictions with a substantially smaller computational effort.

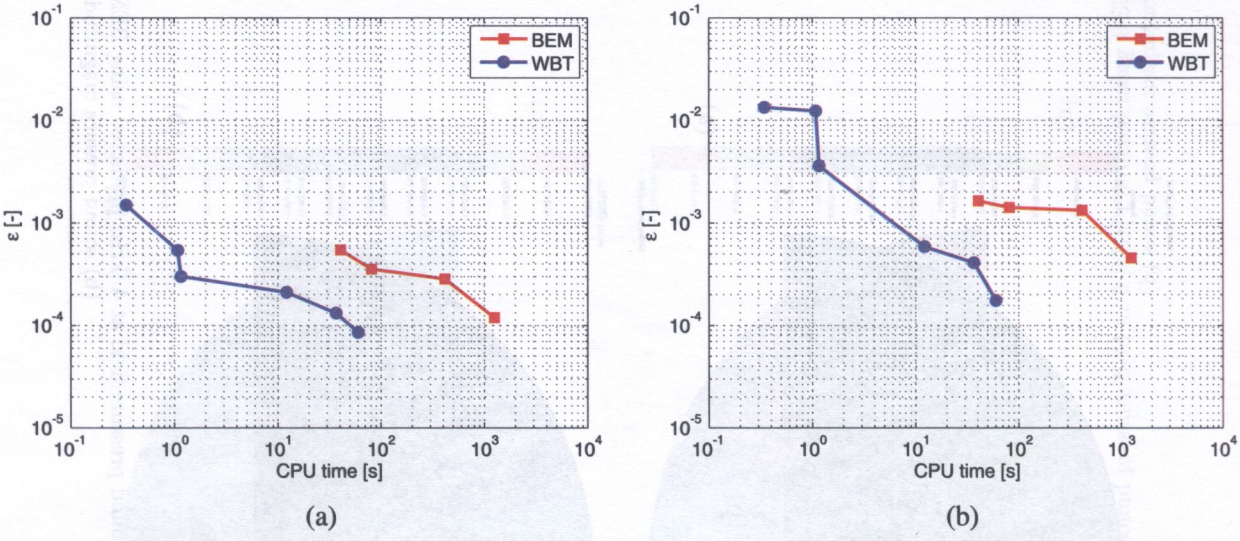

Fig. 8. Pressure convergence curves at (a) 100 [Hz] and (b) 2000 [Hz] calculated using BEM and WBT

Table 2. Properties of the BE models

Model	#nod	#ele	$h_{\max}$[2] [m]	$h_{\min}$[2] [m]	$f_{\max}$[3] [Hz]	CPU time [s]
bem01	1477	2820	0.01	0.005	$\approx$ 2510	40
bem02	2949	5708	0.01	0.002	$\approx$ 2690	80
bem03	4729	9216	0.01	0.001	$\approx$ 2715	410
bem04	8117	15916	0.0035	0.0035	$\approx$ 6500	1235

[2]The maximum/minimum element edge length.
[3]Using the "twelve linear elements per wavelength" rule of thumb.

Table 3. Properties of the WB models

Model	$n_r = n_s = n_t$	L	$\dim\mathbf{\Phi}^b$	$\dim\mathbf{\Phi}^{si}$	$\sum$ DOF	CPU time [s]
wbt01	2	6	54	28	82	0.34
wbt02	4	6	150	28	178	1.07
wbt03	4	8	150	45	195	1.15
wbt04	6	20	294	231	525	12.11
wbt05	8	22	486	276	762	36.42
wbt06	10	25	726	351	1077	59.84

4.2. Patch array

The second validation case considers four rectangular planar radiators mounted in a baffle plane, which form an array having a layout as shown in Fig. 9. Each of the four radiators has the same size of $a = 0.5$ [m] and vibrates piston-like with a normal velocity of $v_n = 0.01$ [m/s]. All four patches radiate in phase. The air has the same material properties as the fluid proposed in the previous case, see Section 4.1.

For the proposed problem, corresponding BE and WB models are constructed. The BE mesh consists of 10400 nodes forming 10000 quadrilateral linear acoustic elements with a maximal element edge length of $h_{\max} = 0.01$ [m], as shown in Fig. 9(a). Again, the baffled direct collocational approach of the LMS/Sysnoise Rev. 5.5 is used to perform the BE calculations. Figure 9(b) depicts the WB model consisting of 14 bounded sub-domains Ω_1–Ω_{14} and one semi-infinite domain Ω_{15} located outside the truncation hemisphere Γ_T, which has the radius of $R = 1.173$ [m]. Each of the subdomains Ω_1–Ω_9 consists of 96 degrees of freedom, subdomains Ω_{10}-Ω_{14} are formed by 150 wave functions each and in the semi-infinite region Ω_{15} 66 wave functions are applied yielding a total number of 1680 wave functions.

Figure 10 shows the comparison of the pressure response predicted by the WBT with a numerical BE solution at a response point $\mathbf{r} = (0.1; 1; 3)$ [m]. Figure 11 captures the distribution of the sound pressure on the baffle plane at 500 [Hz] as predicted with the BE and WB approach, respectively, using an identical color scaling. Again, the WB results are in accordance with the BE predictions.

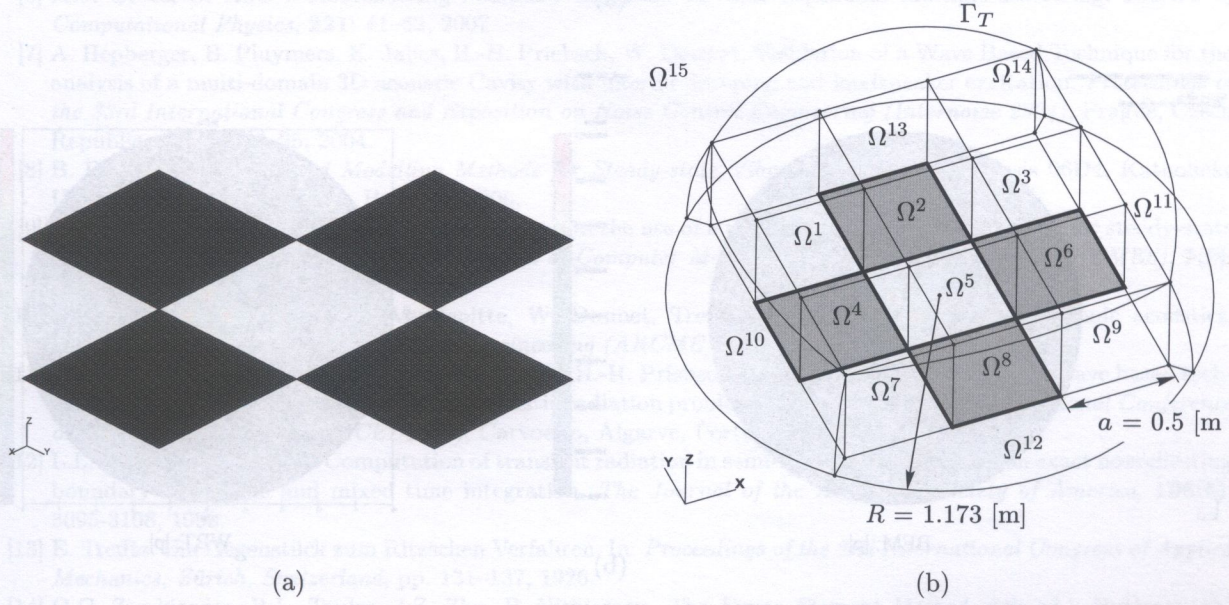

Fig. 9. Patch array: (a) boundary element and (b) a corresponding wave based model

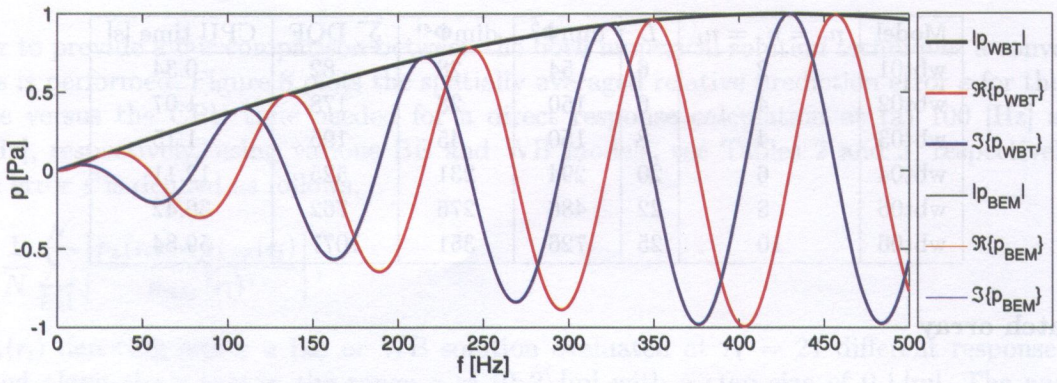

Fig. 10. Patch array: sound pressure responses up to 500 [Hz] evaluated at $\mathbf{r} = (0.1; 1; 3)$ [m]

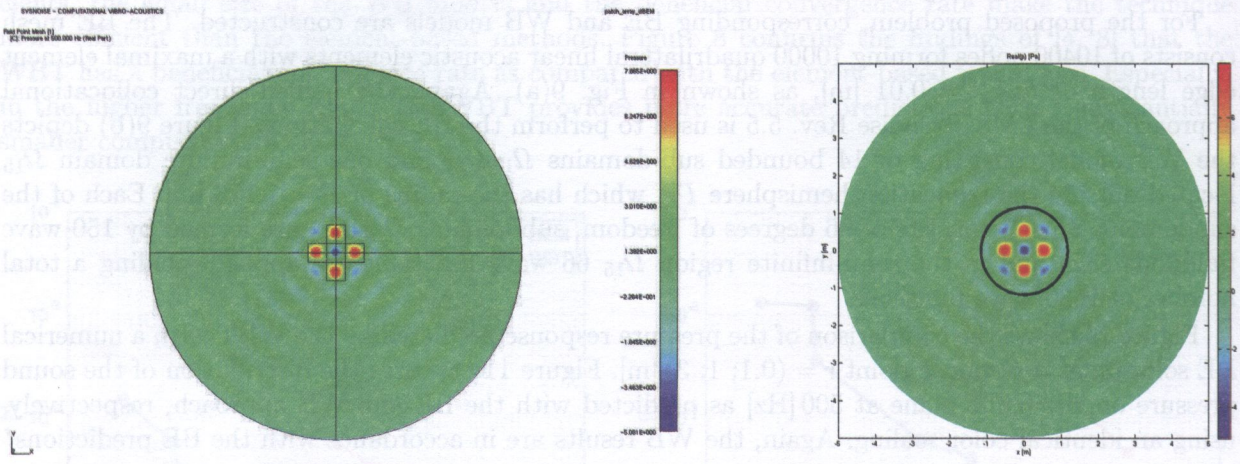

(a)

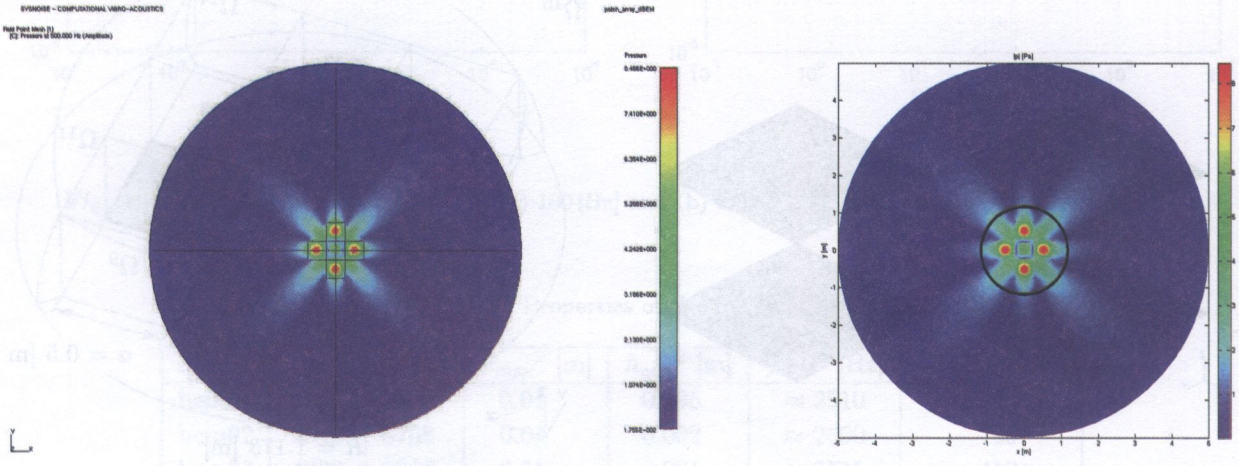

(b)

Fig. 11. Patch array: sound pressure on the baffle at 500 [Hz] predicted using BEM and WBT; (a) real part of the sound pressure [Pa], (b) sound presure magnitude [Pa]

5. Conclusions

This paper applies a recently developed wave based prediction technique for a steady-state sound radiation analysis of three-dimensional problems with semi-infinite domains. It is illustrated through different rigid baffle examples that the wave based technique provides a proper prediction accuracy within a wide frequency range. Furthermore, the comparison with corresponding boundary element models indicates an enhanced convergence rate.

From the practical application point of view, the proposed approach is well suited for the investigations of uncoupled sound radiation problems, e.g. the sound radiation analysis of an engine bay above a road surface. Future research includes an extension of the existing formulation towards semi-infinite fully coupled fluid-structural problems.

Acknowledgements

The research work of Jan Rejlek is funded by the scholarship of the Marie Curie Host Fellowship for Early Stage Research Training (EST), the SIMVIA2 project (EC contract no. MEST-CT-2005-020263), within the Sixth Framework Programme (FP6) of the European Union. The author would like to thank Dr. Franz Diwoky for many valuable hints and inspiring discussions given during this research.

References

[1] R.J. Astley. Infinite elements for wave problems: a review of current formulations and an assessment of accuracy. *International Journal for Numerical Methods in Engineering*, **49**: 951–976, 2000.

[2] J. Berenger. A Perfectly Matched Layer for the Absorption of Electromagnetic Waves. *Journal of Computational Physics*, **114**: 185–200, 1994.

[3] B. Bergen, B. Van Genechten, B. Pluymers, D. Vandepitte, W. Desmet. Efficient wave based models for acoustic scattering and transmission problems using point source and plane wave excitation. *Proceedings of the Fourteenth International Congress on Sound and Vibration (ICSV14)*, Cairns, Australia, July 9–12, 2007.

[4] W. Desmet. *A Wave Based Prediction Technique for Coupled Vibro-acoustic Analysis.* Ph.D. thesis 98D12, Katholieke Universiteit Leuven, Leuven, Belgium, 1998.

[5] O. von Estorff. *Boundary Elements in Acoustics: Advances and Applications.* WIT Press, 2000.

[6] M.J. Grote, C. Kirsch. Nonreflecting boundary condition for time-dependent multiple scattering. *Journal of Computational Physics*, **221**: 41–62, 2007.

[7] A. Hepberger, B. Pluymers, K. Jalics, H.-H. Priebsch, W. Desmet. Validation of a Wave Based Technique for the analysis of a multi-domain 3D acoustic Cavity with interior damping and loudspeaker excitation. *Proceedings of the 33rd International Congress and Exposition on Noise Control Engineering (Internoise 2004)*, Prague, Czech Republic, August 22–25, 2004.

[8] B. Pluymers. *Wave Based Modelling Methods for Steady-state Vibro-acoustics.* Ph.D. thesis 06D4, Katholieke Universiteit Leuven, Leuven, Belgium, 2006.

[9] B. Pluymers, W. Desmet, D. Vandepitte, P. Sas. On the use of a wave based prediction technique for steady-state structural-acoustic radiation analysis. *Journal of Computer Modeling in Engineering & Sciences (CMES)*, **7**(2), 173–184, 2005.

[10] B. Pluymers, B. Van Hal, D. Vandepitte, W. Desmet. Trefftz-based methods for time-harmonic acoustics. *Archives of Computational Methods in Engineering (ARCME)*, **14**: 343–381, 2007.

[11] J. Rejlek, B. Pluymers, F. Diwoky, A. Hepberger, H.-H. Priebsch, W. Desmet. Validation of the wave based technique for the analysis of 2D steady-state acoustic radiation problems. *Proceedings of the International Conference on Engineering Dynamics (ICED2007)*, Carvoeiro, Algarve, Portugal, 2007.

[12] L.L. Thompson, R. Huan. Computation of transient radiation in semi-infinite regions based on exact nonreflecting boundary conditions and mixed time integration. *The Journal of the Acoustical Society of America*, **106**(6): 3095-3108, 1999.

[13] E. Trefftz. Ein Gegenstück zum Ritzschen Verfahren. In: *Proceedings of the 2nd International Congress of Applied Mechanics, Zürich, Switzerland*, pp. 131–137, 1926.

[14] O.C. Zienkiewicz, R.L. Taylor, J.Z. Zhu, P. Nithiarasu. *The Finite Element Method* (6th ed.). Butterworth-Heinemann, 2005.